Structure and Chemical State of Octadecylamine Self-Assembled Monolayers on Mica

ARTICLE *in* THE JOURNAL OF PHYSICAL CHEMISTRY C · SEPTEMBER 2011

Impact Factor: 4.77 · DOI: 10.1021/jp203871g

5 AUTHORS, INCLUDING:

Jose J Benítez
Spanish National Research Council
63 PUBLICATIONS **834** CITATIONS
SEE PROFILE

Miguel San-Miguel
University of Campinas
53 PUBLICATIONS **749** CITATIONS
SEE PROFILE

José Alejandro Heredia-Guerrero
Istituto Italiano di Tecnologia
45 PUBLICATIONS **349** CITATIONS
SEE PROFILE

Miquel Salmeron
University of California, Berkeley
534 PUBLICATIONS **19,736** CITATIONS
SEE PROFILE

THE JOURNAL OF PHYSICAL CHEMISTRY C

Article

pubs.acs.org/JPCC

Electrostatic Induced Molecular Tilting in Self-Assembled Monolayers of *n*-Octadecylamine on Mica

Jaime Oviedo,[†] Miguel A. San-Miguel,[†] José A. Heredia-Guerrero,[‡] and José J. Benítez*[,‡]

[†]Physical Chemistry Department, University of Seville, Seville, Spain

[‡]Materials Science Institute of Seville (ICMS), Spanish Research Council (CSIC) and University of Seville, Americo Vespuccio 49, Isla de la Cartuja, 41092. Seville, Spain

Supporting Information

ABSTRACT: Self-assembled monolayers of *n*-octadecylamine on mica (ODA/mica SAMs) have been investigated by atomic force microscopy (AFM) and by attenuated total reflectance infrared (ATR-FTIR) and X-ray photoelectron (XPS) spectroscopies. Topographic data characterizes a stable configuration with the alkyl skeleton tilted ≈46° from the surface normal that is rationalized according to a well established structural alkyl chain packing model. Extended contact with air increases molecular tilting up to ≈58°. ATR-FTIR and XPS reveal the presence of protonated amino groups within the monolayer and its increment upon exposure to air. The transition between both tilted states is explained assuming the protonation reaction as the driving force and introducing a model to evaluate an electrostatic repulsions term in the overall cohesive energy balance of the system. ODA molecules in the self-assembled monolayer respond to their spontaneous protonation by atmospheric water by tilting as a mechanism to relax the repulsions between $-NH_3^+$ heads.

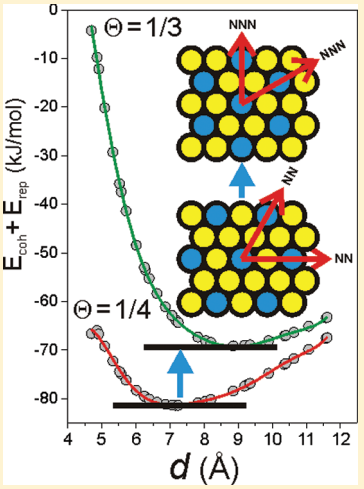

INTRODUCTION

A monolayer of self-assembled molecules (SAM) on a flat surface is a typical example of a well ordered 2D system. The most widely studied are those constituted by linear long chain functionalized alkyl molecules.[1] The technological interest of these systems is based in its consideration as basic steps in a more complex and hierarchical process of nanostructure fabrication.[2] Most of these self-assembled systems are designed by the formation of a strong bond between the molecule and the support to ensure its stability. This is the case of alkythiols on gold and, in a lesser extent, alkylsilanes on silicon. In addition to this, the presence of a metallic or semiconductor support facilitates their integration in conventional lithographic procedures. For these very same reasons, much less attention has been paid to amphiphilic molecules weakly bonded to a nonmetallic support. However, from a fundamental point of view, these are very adequate systems to investigate intermolecular interactions. In the absence of a support driving the structure of molecular packing, 2D ordering is ruled by molecule to molecule interactions, among them van der Waals, electrostatic forces, and hydrogen bonding. Direct structural determination of self-assembled monolayers is commonly attained by high resolution scanning probe microscopies such as scanning tunneling (STM) and atomic force (AFM) microscopies.[3−5] In the particular case of long chain alkyl SAMs weakly adsorbed on a nonconducting support, STM cannot be used. Furthermore, the mechanical effect caused by the scanning tip when operating an AFM microscope in lateral force mode, the usual conditions to obtain atomic resolution, favors the disruption and erosion of the SAMs.

A few years ago, a model describing the molecular packing of linear long chain alkyl molecules in SAMs was proposed.[6−8] It is based on the maximum interlocking of the zigzag arrays of methylene groups between adjacent alkyl chains, and it has explained very successfully the experimentally observed stepwise topographic and frictional changes of alkanethiols on gold and alkylsilanes on Si and mica SAMs under the pressure exerted by the scanning probe. The model predicts the existence of specific tilting angles and monolayer heights, and based exclusively on van der Waals interactions, it estimates the activation energy required for the transition between tilted states.

Due to the above-mentioned difficulties in the structural characterization of weakly adsorbed SAMs, this research takes advantage of the model to study the molecular packing of delicate octadecylamine (ODA) SAMs on mica using the topographic data obtained by AFM. In the particular case of ODA/mica SAMs, there are some experimental observations to be explained. For instance, the monolayer height is significantly shorter if compared with analogous SAMs.[6,8] This suggests a

Received: January 25, 2012
Revised: March 2, 2012
Published: March 6, 2012

   dx.doi.org/10.1021/jp300829g | *J. Phys. Chem. C* 2012, 116, 7099−7105

more tilted configuration despite the associated cohesive energy loss of the packed layer.[9] Second, a characteristic and spontaneous height reduction is systematically observed when ODA/mica SAMs are left in contact with air (ripening) for an extended period of time.[10,11] Progressive amino group ($-NH_2$) protonation and the derived electrostatic repulsion between resulting ($-NH_3^+$) groups was early proposed to explain such height reduction; however, no additional data supporting this hypothesis has yet been provided. To investigate these findings, in this article, we have used ATR-FTIR and XPS to detect and quantify amino protonation and we have introduced an electrostatic repulsive term arising from the presence of protonated amino ($-NH_3^+$) groups in the energy balance of ODA/mica SAMs. To our knowledge, it is the first time that such a study is reported in the literature.

EXPERIMENTAL SECTION

n-Octadecylamine (ODA, $C_{18}H_{37}NH_2$, Fluka >99%) was used as received with no further purification. ODA/mica SAM islands have been prepared by immersing the freshly cleaved mica (muscovite, New York Corp.) pieces in the 15 mM chloroform (Panreac >99.8% stabilized with 50 ppm of amylene) solution for 1 min. They are removed with no rinsing and dried under dry N_2 for 2−3 min. After preparation, samples are allowed to ripen in contact with air for controlled periods of time (from 2 h to 7 days) inside a Petri dish. No specific room humidity control is performed, but it ranges from 45 to 55% RH (temperature calibrated relative humidity HIH Series Honeywell sensor). This article is mainly focused on the study of island topographic changes upon contact with air; thus, though tracking analysis is done along the process, fresh samples, i.e., those analyzed approximately 2 h after preparation, and those extensively ripened (5−7 days) showing the already mentioned height reduction are the most significant. For this reason, both samples are continuously contrasted along the article.

The AFM microscope is a Nanotec "Cervantes" with a 10 μm × 10 μm scanner and connected to a "Dulcinea" electronics. A rectangular Olympus RC800PSA lever with k = 0.1 N/m was employed. For distance calibration, we used a NT-MDT TGT01 silicon grating (2.12 μm pitch) for the X and Y directions and a Nanosensor H8 certified grating with 7.0 nm step height for the Z direction. Images were processed and analyzed using the WSxM software.[12] AFM images were acquired using the so-called "jumping mode" in air at 20−25 °C and 45−55% RH. In this mode, a full approach−retract cycle is completed at every point of the matrix defining an image. Feedback enabling at the contact force set point provides the topographic data, while pull-off forces define the adhesion map. Standard contact mode AFM has been unsuitable for the study of nonripened ODA/mica SAMs, in particular when the scanning size and speed are reduced. ODA/mica SAM islands do need some time, typically several hours, to gain cohesion and resist the mechanical erosion and compression from the tip working in permanent contact. With jumping mode, dragging forces associated to contact and tip displacement in the (X,Y) plane are avoided because rastering is done out of contact.[13] To further prevent mechanical damage, the set point (i.e., the vertical load exerted by the tip on the SAM islands when re-establishing contact) was kept as low as possible. With this type of lever, the force applied to the islands when reestablishing contact is calculated to be around 4.5 nN. 256 lines are acquired in every image at 1 line/s rate. A more detailed description of the AFM acquisition conditions is given elsewhere.[14] Stable and reproducible approach/retract cycling is considered as a reference for the absence of material picking by the probe.

ATR-FTIR spectra have been collected using a PIKE MIRacle ATR accessory (ZnSe crystal plate) attached to a Jasco FT/IR 6200 spectrometer equipped with a MCT detector operating at 4 cm^{-1} resolution. 250 scans have been accumulated in each run using nonpolarized radiation. To prevent interferences arising from the mica support, small pieces were repetitively cleaved to the minimum thickness to allow handling and deposition of *n*-octadecylamine by dipping.[15]

XPS spectra were obtained with a Physical Electronics PHI 5700 spectrometer using nonmonochromatic Mg Kα radiation (300 W, 15 kV, 1253.6 eV) and a multichannel detector. Spectra were recorded in the constant pass energy mode at 29.35 eV with a 720 μm diameter analysis area. Binding energy (BE) values were referred to the methylene C_{1s} peak at 285 eV. C_{1s}, O_{1s}, K_{2p}, and N_{1s} regions have been collected. Particularly, the N_{1s} signal has been analyzed in detail and experimental data have been fitted to Gauss−Lorentz curves with fixed 1.8 eV fwhm using the resident software (PHI Multipack v.8.2B). This bandwidth is extracted from the XPS of bulk ODA containing only the ($-NH_2$) contribution. The relative concentration of N species is calculated from the area of the fitting components. In some cases and to improve the fitting, virtual weak contributions were added to account for some asymmetry on the low and high BE sides of the N_{1s} peak.

EXPERIMENTAL RESULTS

Topographic Characterization of ODA/Mica SAMs. In our experimental conditions, ODA forms rounded, 500−750 nm in diameter and one monolayer thick islands on mica. In such islands, ODA molecules are attached to the surface of mica by the amino group and expose the terminal methyl group, as deduced from friction and adhesion maps.[9,14] When freshly prepared (i.e., ≈2 h old), isolated ODA/mica SAM islands with relatively sharp edges are detected, Figure 1a. Ripening in air causes their progressive contour rounding and aggregation, Figure 1b. However, the most striking observation is the spontaneous island height reduction from an initial 17 Å value to about 13 Å after exposition to the atmosphere for about a week. No such height reduction is observed at periods of aging below 5−7 days. Island flattening is a sudden event, and only in very rare occasions both heights can be observed in the same analysis area (see Figure S1 in the Supporting Information). In both cases, height values are well below the full molecular length (24.6 Å) and, therefore, a configuration in which the alkyl axis is tilted from the surface normal direction is proposed (theoretically 46 and 58°, respectively).

Structural and Chemical Characterization of ODA/Mica SAMs. Use of contact mode AFM has been unsuccessful to obtain molecular resolution images of ODA/mica SAMs.[9] The pressure and dragging exerted by the scanning probe is too high to prevent the displacement of the weakly bonded ODA molecules. This disadvantage has hindered the structural resolution of ODA/mica SAMs packing. We also lack direct structural information of ODA/mica SAMs from diffraction techniques. Consequently, we have to rely on indirect structural data obtained from ATR-FTIR spectroscopy, mostly from the analysis of vibrational modes of methylene ($-CH_2-$) groups.

dx.doi.org/10.1021/jp300829g | J. Phys. Chem. C 2012, 116, 7099−7105

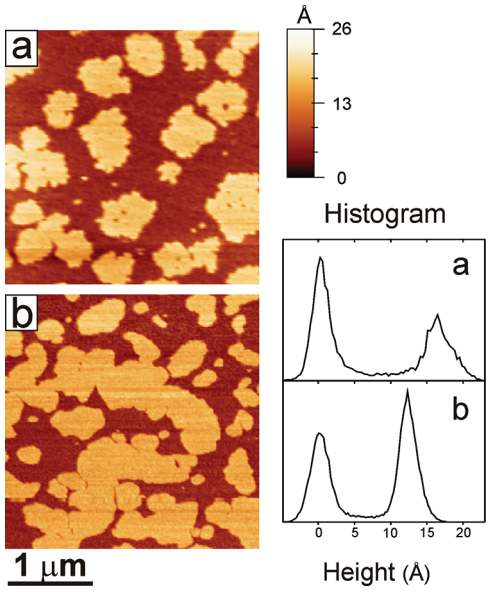

Figure 1. Topographic AFM images of ODA/mica SAM islands prepared from a 15 mM chloroform solution: (a) imaged 2 h after preparation; (b) after 7 days in contact with air. Height histograms (right) show an island height reduction from 17 to 13 Å after such ripening time.

The frequencies of methylene C−H stretching bands of ODA/mica SAMs (ν_a 2917 cm^{-1} and ν_s 2850 cm^{-1}), Figure 2a,

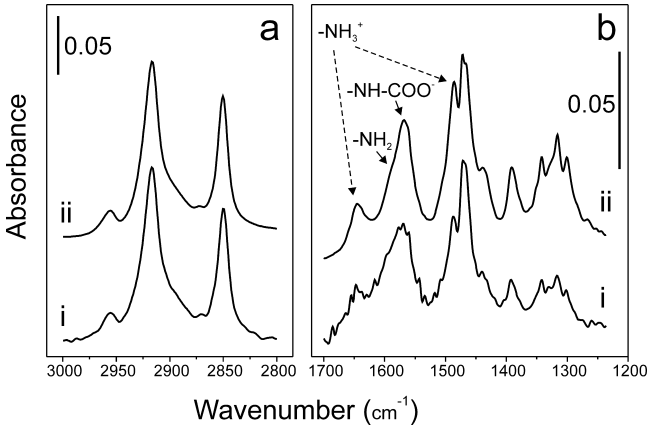

Figure 2. ATR-FTIR spectra of ODA/mica SAMs: (i) 2 h after preparation and (ii) after 7 days ripening in air in (a) the 3000−2800 cm^{-1} and (b) the 1700−1200 cm^{-1} regions. Spectroscopic features indicate a closed packing of alkyl molecules and a slight improvement of ordering with ripening time. In addition to this, the presence of a fraction of octadecylammonium octadecylcarbamate ($-NH-COO^-$) and additional protonated amino groups ($-NH_3^+$) are detected.

are much closer to those reported for crystalline than to the ones corresponding to liquid *n*-alkanes.[16] The peak positions are also very similar to those of solid octadecylamine and well-packed alkyl monolayers.[17,18] Another indication of an ordered, crystal-like structure of ODA/mica SAMs is the splitting of the ($-CH_2-$) scissoring deflection around 1470 cm^{-1}, Figure 2b.[19] The magnitude of the experimental splitting (6 cm^{-1}) is also consistent with a tilted configuration of the alkyl molecules within the crystalline subcell.[18] Finally, the series of methylene twisting−rocking (T) and/or wagging (W) progression bands in the 1350−1250 cm^{-1} region, Figure 2b, are an additional indication of a high degree of chain ordering within the ODA/mica SAM structure.[20,21]

The methylene C−H stretching region displays very slight modifications upon ripening and tilting (i to ii in Figure 2a). No ν_a and ν_s frequency modification is observed; however, a mild peak sharpening (fwhm from 20 to 16 cm^{-1} for ν_a and 12 to 10 cm^{-1} for ν_s) upon aging can be detected. The bandwidth has been related to the molecule mobility within the packed layer,[22] and therefore, a slight improvement of the conformational ordering in the ODA/mica SAMs can be deduced. The same conclusion can be obtained from the enhancement of the methylene twisting−rocking + wagging (T+W) peaks in the 1300−1350 cm^{-1} range, Figure 2b.

The ATR-FTIR spectra of ODA/mica SAMs also contain an intense peak at 1569 cm^{-1}. It is assigned to the deformation and vibration of the ($-NH-COO^-$) group in alkylammonium alkylcarbamates.[23−26] The presence of such carbamate in ODA/mica SAMs is unexpected, but it is confirmed by other peaks at 1645 and 1391 cm^{-1} and by the symmetric deformation of the ($-NH_3^+$) counterion at 1486 cm^{-1}.[27,28] The origin of such octadecylammonium octadecylcarbamate is the fast reaction between ODA molecules and the CO_2 dissolved in the water adlayer formed on the mica surface after cleaving in air.[29]

The N_{1s} XPS spectra of ODA/mica SAMs clearly show the presence of both protonated and nonprotonated amino groups, Figure 3, but there is no direct indication of the carbamate

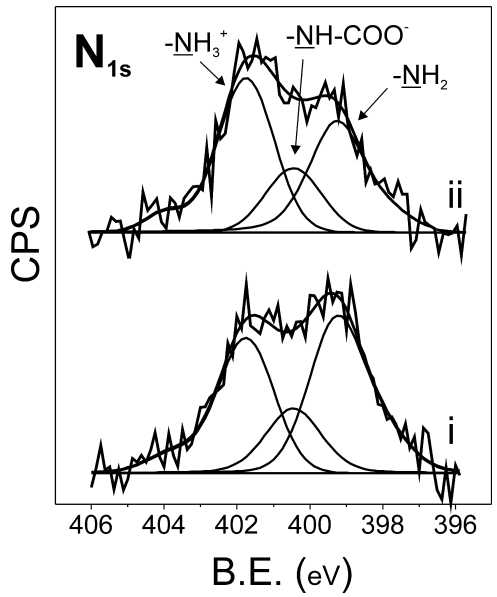

Figure 3. N_{1s} XPS spectra of ODA/mica SAMs exposed to air for (i) 2 h and (ii) 7 days. Contributions of $-NH_3^+$ (401.7 eV), $-NH-COO^-$ (400.4 eV), and $-NH_2$ (399.2 eV) have been extracted. Extended contact with air causes further amino group protonation but no additional carbamation.

phase. However, the detection of this species is so irrefutable from infrared data that a contribution at 400.2 eV ($-NH-COO^-$) has to be added to those at 399.4 and 401.3 eV, respectively assigned to amino ($-NH_2$) and ammonium ($-NH_3^+$) species.[18,26,30−34] The N_{1s} peaks have been fitted using these components, and a progressive increment of the $-NH_3^+/-NH_2$ ratio is observed along the ripening process (see Table S1 and Figure S2 in the Supporting Information).

dx.doi.org/10.1021/jp300829g | J. Phys. Chem. C 2012, 116, 7099−7105

Furthermore, carbamation seems to be constant along the ODA/mica SAM exposition to air, as indicated by the evolution of the 400.2 eV component in Figure 3. However, the presence of protonated amino groups ($-NH_3^+$) is higher than expected from the mere formation of the carbamate (nominal 1:1 $-NH_3^+$:$-NH-COO^-$ ratio). Consequently, it can be concluded that an important fraction (≈20%) of ($-NH_3^+$) is produced by direct amino protonation by the water adlayer at the mica surface at the moment of ODA/mica SAM preparation. After ripening for a week, the concentration of protonated amino groups increases up to about 28% by reaction with extra adsorbed water molecules from moisture. This is corroborated by the increment of the 1486 cm^{-1} peak in the ATR-FTIR spectrum, Figure 2b. The process has been described as the proton transference from water molecules at the edges of islands toward the inside. Steric effects prevent an analogous penetration mechanism for the CO_2 molecule.[29]

Cohesive and Electrostatic Energy Balance in ODA/Mica SAMs. The theoretical packing model proposed by Salmeron et al.[6,8] defines the molecular tilt by the components along the NN (θ_x) and NNN (θ_y) directions of a hexagonal arrangement according to the conditions

$$\tan \theta_x = \frac{na}{s_x} \tag{1}$$

$$\tan \theta_y = \frac{ma}{s_y} \tag{2}$$

where a is the distance (2.5 Å) between alternating C atoms projected along the molecular axis and s_x and s_y the separations, in the perpendicular direction to their alkyl axis, between molecules in the NN (s_x = 4.7 Å) and NNN ($s_y = 3^{1/2}s_x$) directions, respectively. When fully interlocked, n and m are numbers adopting the values

$$n = 0,\ 1/2,\ 1,\ 1\,1/2,\ 2,\ 2\,1/2,\ \ldots \tag{3}$$

$$m = 0,\ 1,\ 2,\ 3,\ \ldots \tag{4}$$

The combination of nearest and next nearest neighbor tilting yields a series of island relative heights (h/L, L = full molecular length) values defining an effective tilting angle (θ). Values for $n \leq 4$ and $m \leq 3$ are compiled in Table 1.

Molecular tilt has a direct effect in the cohesion of the monolayer because end methylene units from both sides of the alkyl chains lose half of their matching counterparts, Figure 4.

Table 1. Molecular Tilting Angle from the Surface Normal (θ) Predicted from the Structural Model Proposed by Salmeron et al.

	cos θ			
n	m = 0	m = 1	m = 2	m = 3
0	1	0.956	0.852	0.735
1/2	0.966	0.923	0.823	0.710
1	0.883	0.844	0.752	0.649
1 1/2	0.782	0.748	0.666	0.575
2	0.685	0.655	0.584	0.503
2 1/2	0.601	0.575	0.512	0.442
3	0.531	0.508	0.452	0.390
3 1/2	0.475	0.454	0.405	0.349
4	0.425	0.406	0.362	0.312

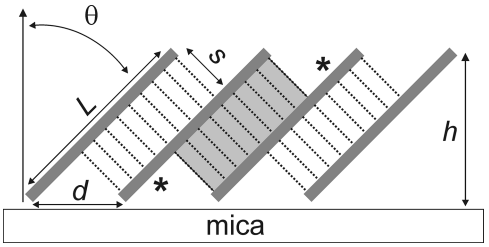

Figure 4. Schematic drawing illustrating the reduction of lateral molecule to molecule interactions in a self-assembled monolyer upon tilting (θ). The asterisks indicate the methylene ($-CH_2-$) groups having no counterparts on one side.

To evaluate the cohesive energy dependence upon tilting, we have defined an overlapping factor (F) defined as

$$F = 1 - \frac{s \tan \theta}{L} \tag{5}$$

where s is the chain to chain separation in the packed structure (4.7 Å) and L the full n-octadecylamine molecular length (24.6 Å). We have considered the cohesive energy to be proportional to the effective overlapping between alkyl chains (F), being E_{coh} = 129.5 kJ/mol when fully vertical (F = 1). This energy value has been obtained from C_{18} alkane sublimation energy.[35] Considering the discrete tilting angles of Table 1 and the corresponding overlapping factors (F), we have constructed a curve predicting the evolution of the cohesive energy (E_{coh}) with tilting, Figure 5a. In this case, inclination is represented by the head to head distance (d) along a direction parallel to the plane support ($d = s/\cos \theta$). As observed, a continuous decrease of cohesive energy vs d is postulated.

To estimate the electrostatic repulsion energy, we have represented the protonation of ODA molecules in the SAM as the association of hydroxyl groups and $-NH_3^+$ cations. Such ion pair would define a dipole. Because of the superimposed SAM packing symmetry, all dipoles are considered to be parallel. Besides, and due to the dynamic character of molecules in this weakly adsorbed system, we postulate that dipoles should be uniformly distributed to minimize electrostatic repulsions. XPS reveals that the percentage of amino groups protonated by water is about 20% when freshly prepared and ≈28% after ripening for a week. In our model, these protonation states are represented by two homogeneous distributions considering protonated molecules along the NN (Θ = 1/4) and NNN (Θ = 1/3) directions, Figure 6. This would yield a theoretical 25 and 33% amine protonation, respectively, very similar to the experimental values indicated.

The interaction energy between two parallel dipoles can be expressed as

$$U = \frac{p^2}{4\pi\varepsilon_r\varepsilon_o}\frac{1}{D^3} \tag{6}$$

where p is the dipole moment, ε_o and ε_r the vacuum and the relative dielectric permittivities, respectively, and D the distance between dipoles. Expanding the interaction to every shell containing N_i dipoles located at distances D_i and expressing D as a function of the effective radius R of the packed dipoles (Figure 6):

$$U = \frac{1}{4\pi\varepsilon_o}\left(\frac{p^2}{\varepsilon_r}\right)\frac{C}{R^3} \tag{7}$$

dx.doi.org/10.1021/jp300829g | J. Phys. Chem. C 2012, 116, 7099−7105

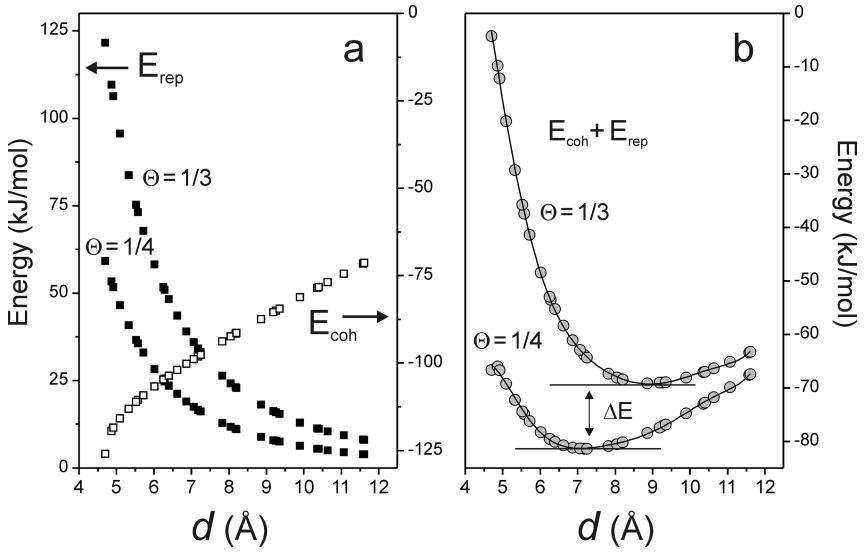

Figure 5. (a) Electrostatic repulsion (E_{rep}) and cohesive (E_{coh}) energy dependence with the molecular head to head separation (d) and protonation fraction (Θ) derived from the models proposed for ODA/mica SAMs. (b) Cohesive-repulsion energy balance for the Θ = 1/4 and Θ = 1/3 configurations, energy minima at $d \approx 7$ Å and $d \approx 9$ Å are detected, respectively.

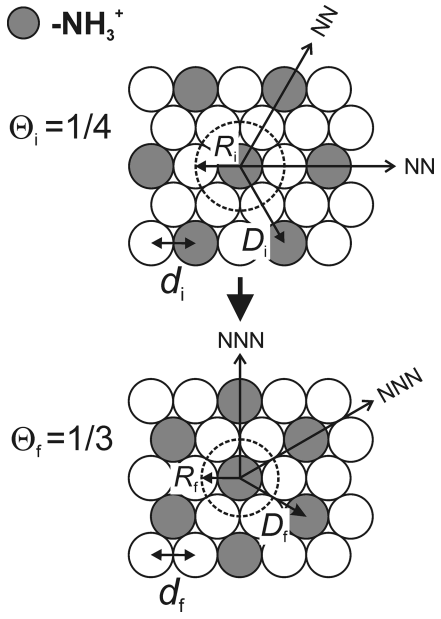

Figure 6. Hexagonal molecular packing models (at the support plane) proposed for the uniform distributions of protonated ODA molecules within the SAM. Theoretic protonation fractions (Θ) are selected according to XPS results for freshly prepared (Θ = 1/4) and ripened (Θ = 1/3) ODA/mica SAMs.

where C is a constant obtained by convergence of the additive series (C = 1.3764641) (see the Supporting Information). If we express the energy values in kJ/mol and divide by a factor of 2 to avoid counting the same interaction twice, the repulsion interaction between dipoles in a close packed hexagonal arrangement with a dipole fraction (Θ) can be written as

$$U\ (\mathrm{kJ\ mol^{-1}}) = 415\left(\frac{p^2}{\varepsilon_r}\right)\frac{\Theta}{R^3} \tag{8}$$

where R is indicated in angstroms and p in debyes (1 D = 3.33564 × 10^{-30} C m). To compare with cohesive energy values, U will be expressed as a function of d, the head to head distance. For the Θ = 1/4 arrangement, $R = d$, and for Θ = 1/3, $R = d3^{1/2}/2$, Figure 6; thus,

$$U(\Theta = 1/4) = 103.75\left(\frac{p^2}{\varepsilon_r}\right)\frac{1}{d^3} \tag{9}$$

and

$$U(\Theta = 1/3) = 212.98\left(\frac{p^2}{\varepsilon_r}\right)\frac{1}{d^3} \tag{10}$$

Separation between ($-NH_3^+$) cations and hydroxyl anions (OH^-) is set as 3 Å, the sum of ionic radii of ammonium (1.50 Å) and hydroxyl ions (1.54 Å). This would yield p values of about 14.4 D. Assuming a dielectric constant (ε_r = 3.5)[36] and the set of head to head separation (d) values corresponding to the tilted states indicated in Table 1, electrostatic repulsion energy (E_{rep}) vs d curves have been constructed, Figure 5a. The energy balance between cohesion and electrostatic repulsion (E_{coh} + E_{rep}) for both Θ = 1/4 and Θ = 1/3 is also indicated, Figure 5b. As observed, energy minima develop for both configurations and equilibrium head to head distances of about 7 and 9 Å are obtained for Θ = 1/4 and Θ = 1/3, respectively. Such distances correspond to relative height values (h/L) of 0.67 and 0.52 in quite good agreement with the 0.69 (h = 17 Å) and 0.53 (h = 13 Å) experimental data for the freshly prepared and the ripened ODA SAMs, respectively, Figure 1.

DISCUSSION

AFM topographic data indicates that ODA/mica SAMs form a highly packed and ordered molecular structure with the alkyl skeleton tilted with respect to the surface normal. ATR-FTIR provides additional experimental evidence supporting this finding via the methylene stretching and deflection peaks. Molecular tilts derived from experimental height values, Figure 1, do match the n = 2 and n = 3 tilting states (47 and 58° from the surface normal, respectively) defined by the close packing model reported by Salmeron et al.[6−8] Such inclination is much higher than the ones observed for similar SAMs of alkyl-silanes and thiols,[6,8] which is intriguing because island cohesive energy

dx.doi.org/10.1021/jp300829g | J. Phys. Chem. C 2012, 116, 7099−7105

is lost upon tilting. To address this issue, we have revised the literature on octadecylamine specific surface areas obtained from Langmuir−Blodgett isotherms. Didymus et al.[37] have reported values of 20−22 Å^2/molecule. Taking into account the surface packing density factor ($\pi/\sqrt{12}$), the amino to amino separation (d) in a closed hexagonal packing calculated from such specific surface areas is 4.8−5.0 Å. This is slightly above the predicted 4.7 Å for the fully vertical $n = 0$ state, so it can be deduced then that mere steric repulsions between unprotonated $-NH_2$ head groups already prevents the formation of such ($n = 0$) phase. At low subphase pH (pH 3), at which full $-NH_2$ protonation is expected, the specific area increases up to 30−35 Å^2/molecule.[37] This means a higher headgroup separation (about 5.9−6.4 Å) arising from the electrostatic repulsions between protonated amino groups ($-NH_3^+$). The nominal (d) value for the next tilted state $n = 1$ is 5.3 Å. Though amino group protonation is only partial in ODA/mica SAMs, it is assumable that the 5.3 Å value is too close to the limiting 4.8−5.0 Å separation to make the $n = 1$ be a stable configuration when an electrostatic repulsion component develops. These qualitative considerations seem to explain why the tilted $n = 2$ state ($d = 6.9$ Å, $\theta \approx 47°$) is systematically observed upon ODA/mica SAM preparation. Our work introduces a more quantitative argument based on the balance between cohesive and electrostatic repulsion energy. Thus, at short periods of contact with air ($\Theta = 1/4$), the model predicts a stable configuration at separation values (d) around 7 Å, Figure 5b, which is in good agreement with our experimental topographic AFM data.

Apart from island rounding, displacement, and coalescence into bigger ones, the ODA/mica SAM height reduction and the increment of protonation percentage are the only experimental observations caused by extended ripening. Consequently, we have related both phenomena. Amine protonation in solution is an exothermic reaction with reported enthalpy values of about 60 kJ/mol[38] and can be considered then as the driving force for the process. The progressive incorporation of water molecules to the $-NH_2$/mica interface would displace the equilibrium toward protonation. The resulting increment of charge density in the confined structure of the ODA/mica SAM is accompanied by an increase of the electrostatic repulsions, and to accommodate the charge increment, the system reacts by separating them and reaching the $\Theta = 1/3$ state, Figure 6. Separation is achieved by a stepwise alkyl chain to chain sliding and the transition to the next allowed tilted configuration ($n = 2$ to $n = 3$). Under these conditions, the new cohesive-repulsive energy balance is represented by the $\Theta = 1/3$ curve in Figure 5b and predicts a head to head separation (d) of ≈9 Å, in good agreement with the one calculated from experimental AFM data.

From the curves in Figure 5b, the $n = 2$ to $n = 3$ transition needs $\Delta E \approx 12$ kJ on going from a protonation percentage of 25 to 33.3%. This would require a process supplying about 140 kJ/mol, which is a higher value but in the order of magnitude of the amine protonation enthalpy reported. In addition to this, it should be taken into account that mica surfaces carry a negative charge and the incorporation of positively charged groups provides an additional electrostatic energy that may contribute to the $n = 2$ to $n = 3$ transition.

CONCLUSIONS

Extended contact with air (ripening) is an important parameter influencing the topography of weakly adsorbed self-assembled monolayers of *n*-octadecylamine on mica. The spontaneous protonation of weak basic amino groups induced by atmospheric water introduces significant electrostatic repulsions between molecules in such a confined structure. Starting from a well established model describing the close packing of alkyl chains in SAMs, the contributions of the electrostatic repulsions have been evaluated using dipole to dipole interactions. The balance between cohesive and repulsion energy as a function of the head to head separation in ODA/mica SAMs shows a series of minima that can be assigned to experimentally observed tilted configurations. Tilting, and the consequent head to head separation, is the response of the packed system to relax such electrostatic repulsions. The model proposed predicts an energy gap for the transition between tilted configurations in the order of magnitude of the driving process: the amine protonation by water.

ASSOCIATED CONTENT

Supporting Information

AFM data showing the coexistence of the $h \approx 17$ Å and the $h \approx 13$ Å phases in a *n*-octadecylamine self-assembled monolayer on mica; XPS data on the progressive protonation of ODA molecules along ripening; the algorithm to calculate the convergence constant (C) in the electrostatic repulsion energy calculation. This material is available free of charge via the Internet at http://pubs.acs.org.

AUTHOR INFORMATION

Corresponding Author

*E-mail: benitez@icmse.csic.es. Phone: 34 954489551. Fax: 34 954460665.

Notes

The authors declare no competing financial interest.

ACKNOWLEDGMENTS

Funding is provided by the Spanish Ministerio de Ciencia e Innovación under project CTQ2008-00188.

REFERENCES

(1) Ulman, A. *Chem. Rev.* **1996**, *96*, 1533−1554.
(2) Whitesides, G. M; Grzybowski, B. *Science* **2002**, *295*, 2418−2421.
(3) Widrig, C. A.; Alves, C.; Porter, M. D. *J. Am. Chem. Soc.* **1991**, *113*, 2805−2810.
(4) Alves, C. A.; Smith, E. L.; Porter, M. D. *J. Am. Chem. Soc.* **1992**, *114*, 1222−1227.
(5) Liu, G-y.; Fenter, P.; Chidsey, C. E. D.; Ogletree, D. F.; Eisenberger, P.; Salmeron, M. *J. Chem. Phys.* **1994**, *101*, 4301−4306.
(6) Barrena, E.; Kopta, S.; Ogletree, D. F.; Charych, D. H.; Salmeron, M. *Phys. Rev. Lett.* **1999**, *82*, 2880−2883.
(7) Würger, A. *Phys. Rev. Lett.* **1999**, *83*, 1696.
(8) Barrena, E.; Ocal, C.; Salmeron, M. *J. Chem. Phys.* **2000**, *113*, 2413−2418.
(9) Benítez, J. J.; Kopta, S.; Ogletree, D. F.; Salmeron, M. *Langmuir* **2002**, *18*, 6096−6100.
(10) Benítez, J. J.; Kopta, S.; Díez-Pérez, I.; Sanz, F.; Ogletree, D. F.; Salmeron, M. *Langmuir* **2003**, *19*, 762−765.
(11) Benítez, J. J.; Salmeron, M. *J. Chem. Phys.* **2006**, *125*, 044708.
(12) Horcas, I.; Fernandez, R.; Gomez-Rodriguez, J. M; Colchero, J.; Gomez-Herrero, J.; Baro, A. *Rev. Sci. Instrum.* **2007**, *78*, 013705.
(13) de Pablo, P. J.; Colchero, J.; Gómez-Herrero, J.; Baró, A. M. *Appl. Phys. Lett.* **1998**, *73*, 3300−3302.
(14) Benítez, J. J.; Heredia-Guerrero, J. A.; Salmeron, M. *J. Phys. Chem. C* **2010**, *114*, 12630−12634.

(15) Guzonas, D. A.; Hair, M. L.; Tripp, C. P. *Appl. Spectrosc.* **1990**, *44*, 290−293.
(16) Snyder, R. G.; Strauss, H. L.; Elliger, C. A. *J. Phys. Chem.* **1982**, *86*, 5145−5150.
(17) Hostetler, M. J.; Stokes, J. J.; Murray, R. W. *Langmuir* **1996**, *12*, 3604−3612.
(18) Chernyshova, I. V.; Hanumantha Rao, K.; Vidyadhar, A.; Shchukarev, A. V. *Langmuir* **2000**, *16*, 8071−8084.
(19) Snyder, R. G. *J. Mol. Spectrosc.* **1961**, *7*, 116−144.
(20) Smith, E. L.; Porter, M. D. *J. Phys. Chem.* **1993**, *97*, 8032−8038.
(21) Snyder, R. G. *J. Chem. Phys.* **1967**, *47*, 1316−1360.
(22) Katayama, N.; Enomoto, S.; Sato, T.; Ozaki, Y. *J. Phys. Chem.* **1993**, *97*, 6880−6884.
(23) Gaines, G. L. *Nature* **1982**, *298*, 544−545.
(24) Aresta, M.; Quaranta, E. *Tetrahedron* **1992**, *48*, 1515−1530.
(25) Holas, T.; Zbytovska, J.; Vavrova, K.; Berka, P.; Madlova, M.; Klimentova, J.; Hrabalek, A. *Thermochim. Acta* **2006**, *441*, 116−123.
(26) Luo, B.; Rossini, J. E.; Gladfelter, W. L. *Langmuir* **2009**, *25*, 13133−13141.
(27) Pohle, W.; Gauger, D. R. *J. Mol. Struct.* **2009**, *924*−*926*, 144−147.
(28) Nakanishi, K.; Goto, T.; Ohashi, M. *Bull. Chem. Soc. Jpn.* **1957**, *30*, 403−408.
(29) Benítez, J. J.; San-Miguel, M. A.; Domínguez-Meister, S.; Heredia-Guerrero, J. A.; Salmeron, M. *J. Phys. Chem. C* **2011**, *115*, 19716−19723.
(30) Himmel, H. J.; Kaschke, M.; Harder, P.; Wöll, Ch. *Thin Solid Films* **1996**, *284*−*285*, 275−280.
(31) Nora, G; Yegen, E.; Gross, T.; Lippitz, A.; Weigel, W.; Krakert, S.; Terfort, A.; Unger, W. E. S. *Surf. Sci.* **2009**, *603*, 2849−2860.
(32) Kumar, A.; Mandal, S.; Selvakannan, P. R.; Pasricha, R.; Mandale, A. B.; Sastry, M. *Langmuir* **2003**, *19*, 6277−6282.
(33) Matsuo, Y.; Miyabe, T.; Fukutsuka, T.; Sugie, Y. *Carbon* **2007**, *45*, 1005−1012.
(34) Chmielewska, E.; Tylus, W. In *Combined and Hybrid Adsorbents*; Loureiro, J. M., Kartel, M. T., Eds.; Springer: Dordrecht, The Netherlands, 2006; pp 63−70.
(35) Israelachvili, J. *Intermolecular and Surface Forces*; Academic Press: New York, 1991; p 89.
(36) Wohlfarth, C. In *Handbook of Chemistry and Physics*, 87th ed.; Lide, D. R., Ed.; CRC Press: Boca Raton, FL, 2006; Sec. 6, pp 132−153.
(37) Didymus, J. M.; Mann, S.; Benton, W. B.; Collins, I. R. *Langmuir* **1995**, *11*, 3130−3136.
(38) Paoletti, P.; Barbucci, R.; Vacca, A. *J. Chem. Soc., Dalton Trans.* **1972**, *18*, 2010−2013.